Magnetic moment distribution in NiMn alloys*

J. W. Cable and H. R. Child
Solid State Division, Oak Ridge National Laboratory, Oak Ridge, Tennessee 37830
(Received 1 July 1974)

Polarized-neutron diffuse-scattering measurements were made on Ni-rich NiMn alloys to determine the distribution of magnetic moments in this system. At 5-at.% Mn, the individual moments are $(3.50 \pm 0.13)\mu_B$/Mn and $(0.584 \pm 0.013)\mu_B$/Ni assuming no conduction-electron polarization. Both moments decrease with increasing Mn content and attain values of $(1.10 \pm 0.04)\mu_B$/Mn and $(0.300 \pm 0.013)\mu_B$/Ni at 20-at.% Mn. Near-neighbor magnetic-moment correlations appear in the scattering functions simultaneously with the decrease in moments, and, since the cross sections are dominated by the Mn contribution, this indicates that the ferromagnetically aligned Mn moment is strongly dependent on near-neighbor environment. The actual moment dependence on environment was not determined but this is not simply a matter of the number of Mn nearest neighbors as has been assumed in previously proposed competing interaction models. The Mn and Ni moments exhibit different relative magnetization behavior with a stronger temperature dependence for the Mn moment. This behavior is consistent with the quasi-independent local-moment model with an impurity-host to host-host coupling ratio of about 0.3.

I. INTRODUCTION

The magnetic behavior of NiMn alloys provides a classical example of a system with competing interactions. The magnetization of the quenched alloys increases linearly with Mn content to about 6% Mn, reaches a maximum at 10% Mn, and then decreases rapidly above 10% Mn and approaches zero near 25% Mn.[1-5] Above 15% Mn the magnetization becomes order dependent with the most dramatic effects occurring in the 25%-Mn region. (Here, and throughout this paper, the Mn content is expressed in atomic percent.) This anomalous behavior has been interpreted in terms of a nearest-neighbor molecular-field model with antiferromagnetic MnMn and ferromagnetic NiNi and NiMn interactions.[6] According to this model, the magnetic moment at a given Mn site aligns parallel or antiparallel to the Ni moments depending on the net effective field exerted by the nearest-neighbor environment of that atom. Alternatively, the competing interactions might lead to a canting of the Mn moments rather than to spin reversal.[7-9] In either case the composition and order dependence of the magnetization can be reproduced with properly selected parameters. If such Mn-moment fluctuations with near-neighbor environment actually occur, then the magnetic diffuse scattering of neutrons from these alloys should exhibit a K dependence characteristic of these spatial-moment correlations. No such K dependence was observed in previously reported neutron measurements,[10] but these were made with unpolarized neutrons for which the magnetic diffuse cross sections are quite small. We report here the results of measurements carried out with polarized neutrons for which an order-of-magnitude enhancement of the cross section is obtained. Some of these results were described earlier.[11]

II. EXPERIMENT

With incident neutrons polarized parallel and antiparallel to the sample magnetization and perpendicular to the scattering vector, the magnetic disorder scattering from a binary ferromagnetic alloy is given by

$$\frac{d\sigma^{\pm}}{d\Omega}(K) = c(1-c)\,S(K)\,(\Delta b \pm \Delta p)^2 . \tag{1}$$

Here, c is the fractional solute content, Δb and Δp are the differences in nuclear and magnetic scattering amplitudes of the constituents, and the $\pm$ sign refers to parallel and antiparallel polarization. The magnetic amplitude difference is related to the moment difference by

$$\Delta p = 0.2695\, f(K)\, \Delta\mu , \tag{2}$$

in which $f(K)$ is an appropriate form factor. For polycrystalline samples, the scattering function is

$$S(K) = 1 + \sum_i z_i\, \alpha(R_i)\, \frac{\sin KR_i}{KR_i} , \tag{3}$$

in which z_i is the number of neighbors in the ith shell and the α's are short-range-order (SRO) parameters defined by

$$\alpha(R_i) = 1 - P^{AB}(R_i)/c_A . \tag{4}$$

Here, $P^{AB}(R_i)$ is the probability of finding an A atom at distance R_i from a B atom. The sum and the difference of the two cross sections are

$$\sum \frac{d\sigma}{d\Omega} \equiv \frac{1}{2}\left(\frac{d\sigma^{+}}{d\Omega} + \frac{d\sigma^{-}}{d\Omega}\right) = c(1-c)\,S(K)\,(\Delta b^2 + \Delta p^2) \tag{5}$$

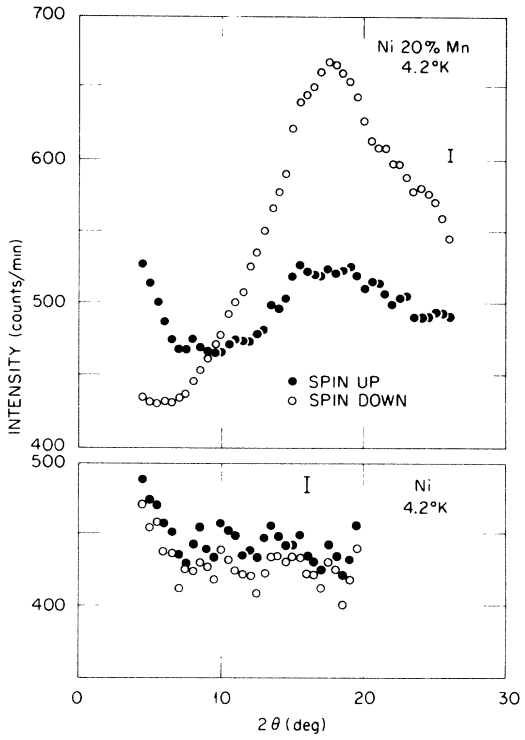

FIG. 1. Diffuse scattering of polarized neutrons from pure Ni and from a Ni–20-at.%-Mn alloy at 4.2 °K.

and

$$\Delta \frac{d\sigma}{d\Omega} \equiv \frac{d\sigma^+}{d\Omega} - \frac{d\sigma^-}{d\Omega}$$

$$= 4c(1-c)S(K)\,\Delta b\,\Delta p\,, \qquad (6)$$

and these should have the same $S(K)$ dependence if the binary model applies to the system. However, if there are moment variations with local environment, then the binary model is not appropriate and $\sum (d\sigma/d\Omega)$ and $\Delta (d\sigma/d\Omega)$ may have quite different K dependences.

III. EXPERIMENTAL RESULTS

A. 4.2 °K

Polarized-neutron diffuse-scattering measurements were made for Ni and for NiMn alloys containing from 5 to 20 at.% Mn. The samples were polycrystalline plates of 2-mm thickness which had been machined from arc-melted drop-cast ingots, annealed for 24 h at 1000 °C and then quenched to room temperature. Electron probe and x-ray analyses showed them to be macroscopically homogeneous and single-phase fcc with lattice parameters in good agreement with the literature values. The samples were mounted in the polarized neutron spectrometer in symmetrical transmission geometry with a vertical magnetizing field. The diffuse intensity inside of the first Bragg reflection was measured with incident neutrons polarized parallel (spin-up) and antiparallel (spin-down) to the applied field. The marked spin dependence of the scattering is illustrated in Fig. 1, which shows the scattered intensity of spin-up and spin-down neutrons from pure Ni and from a Ni–20% Mn alloy at 4.2 °K in a magnetizing field of 20 kOe. For pure Ni this intensity contains contributions from incoherent, thermal diffuse, and multiple Bragg scattering. Of these, only the last is spin dependent, and the different scattered intensities for the two spin states merely reflect the more effective Bragg scattering of spin-up neutrons. The scattered intensity from the alloy contains these three terms plus the spin-dependent disorder scattering described in Sec. II. Clearly, the disorder scattering is the dominant spin-dependent effect for this system.

The observed intensities were corrected for instrumental background, incomplete incident polarization (< 1%), and sample depolarization (~1%) and converted to absolute cross sections by calibration with a standard V scatterer. The resulting sum and difference cross sections are shown in Figs.

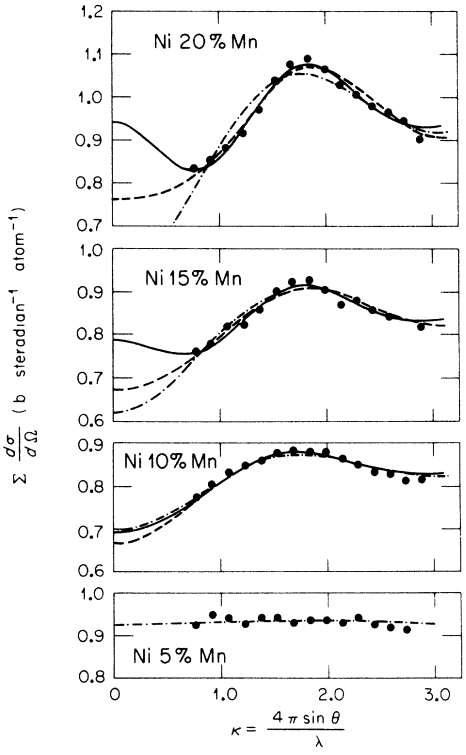

FIG. 2. Sum cross sections at 4.2 °K. Fitted curves are for one (-•--•), two (- - -) and three (———) SRO parameters. Mn content shown for each data set is atomic percent.

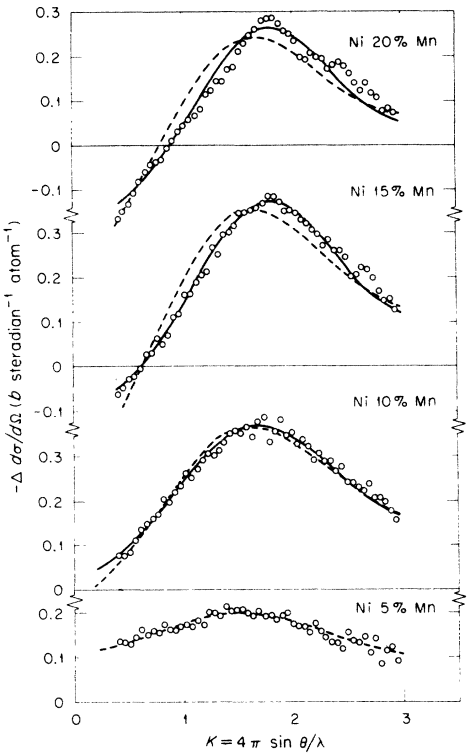

FIG. 3. Difference cross sections at 4.2°K. Dashed and solid curves are fitted with one and two order parameters, respectively. Mn content shown for each data set is atomic percent.

2 and 3.

The sum cross sections have been corrected for the thermal diffuse scattering, which is small and readily calculable, but still contain the incoherent and multiple Bragg terms which we assume are independent of K. Since Δb^2 is typically an order of magnitude larger than Δp^2 for this system, we neglect the Δp^2 term in Eq. (5) and fit, by the method of least squares, the observed sum cross sections to the equation

$$\sum \frac{d\sigma}{d\Omega}(K) = C + c_{\mathrm{Ni}}\, c_{\mathrm{Mn}}\, \Delta b^2 S(K)\ , \qquad (7)$$

with fitting parameters C and $\alpha(R_i)$. The fitted curves are shown in Fig. 2 and the corresponding SRO parameters are given in Table I as a function of the number of SRO parameters included in the fit. Here, the rms deviation of the fit is in millibarns/(data point) and this should be compared with the statistical error of ±4 mb/(data point). The SRO parameters are small and essentially independent of the number of parameters included. Only for the 20%-Mn alloy does inclusion of a second-neighbor parameter significantly improve the fit. At this composition the negative $\alpha(R_1)$ and positive $\alpha(R_2)$ values are consistent with the Cu_3Au type of order that develops in this system near 25% Mn. We note that these SRO parameters should be taken with some caution since they are obtained from polycrystalline data over a limited region of K space. Nevertheless, they are adequate for our purpose here, since we are primarily interested in a comparison of the $S(K)$ functions from $\sum(d\sigma/d\Omega)$ and $\Delta(d\sigma/d\Omega)$. As can be seen by reference to Fig. 2, the shape of $S(K)$ in the region where data were obtained is largely determined by $\alpha(R_1)$.

For the difference cross sections the instrumental background, incoherent and thermal diffuse scattering cancel in taking the difference. Multiple-Bragg-scattering corrections are required and these were calculated by standard methods,[12] using the observed spin-dependent transmissions. Although these calculations are only approximate, a measure of their reliability is provided by the observed effect in pure Ni. Measurements were made on four different samples of Ni which had been heat treated in the same way as the alloy samples. The observed multiple-Bragg-scattering effect showed no K dependence for any of the samples and varied in magnitude from 30 to 52 mb while the calculated effect was 46 mb. The calculated corrections for the alloys vary from about 50 mb at 5% Mn to 10 mb at 20% Mn. The corrected $\Delta(d\sigma/d\Omega)$ were fitted to Eq. (6) with parameters $\alpha(R_i)_{\mathrm{mag}}$ and $\Delta p(0)$, the magnetic scattering amplitude difference at $K = 0$. This requires a form-factor assumption and we have used $f(K) = e^{-0.069K^2}$, which closely approximates the Mn^{+2} form factor over the present region of K. The fitted curves and the corresponding parameters are given in Fig. 3 and Table II. Comparison of Tables I and II shows two regions of magnetic behavior for these alloys. Below 10% Mn, $\Delta p(0)$ is large and $\alpha(R_1) \simeq \alpha(R_1)_{\mathrm{mag}}$. The binary model is valid in this

TABLE I. Positional SRO parameters of NiMn alloys.

At.% Mn	$\alpha(R_1)$	$\alpha(R_2)$	$\alpha(R_3)$	rms dev. (mb)
5	−0.01	−0.03	−0.01	2.4
	−0.01	−0.03		2.5
	−0.01			2.5
10	−0.06	−0.03	+0.01	2.4
	−0.07	−0.03		2.4
	−0.07			2.5
15	−0.07	+0.01	+0.02	2.9
	−0.08	+0.03		3.5
	−0.08			3.8
20	−0.09	+0.07	+0.02	3.3
	−0.10	+0.09		4.3
	−0.10			6.8
	±0.02	±0.04	±0.02	

TABLE II. Magnetic-cross-section parameters of NiMn alloys at 4.2 °K.

At.% Mn	$\Delta p(0)$	$\alpha(R_1)_{mag}$	$\alpha(R_2)_{mag}$	$\alpha(R_3)_{mag}$	rms dev. (mb)
5	0.786	−0.04	−0.03	+0.01	1.6
	0.786	−0.04	0.00		1.7
	0.785	−0.04			1.7
10	0.715	−0.10	+0.06	−0.01	1.7
	0.715	−0.09	+0.04		1.8
	0.712	−0.08			2.4
15	0.448	−0.17	+0.14	−0.01	2.2
	0.448	−0.16	+0.12		2.3
	0.443	−0.14			4.8
20	0.215	−0.26	+0.27	−0.02	2.9
	0.216	−0.25	+0.19		3.1
	0.212	−0.20			5.1

region. Above 10% Mn, $\Delta p(0)$ decreases sharply with Mn content and $\alpha(R_1) \neq \alpha(R_1)_{mag}$. The large values of $\alpha(R_1)_{mag}$ indicate a breakdown of the binary model in this region and magnetic correlations at nearest-neighbor distances. The simultaneous occurrence of these correlations with a decreasing $\Delta p(0)$ suggests a moment reorientation as in the competing-interaction models. We now consider the cross sections to be expected for such models.

We consider a model in which the Mn moment is a function of n, the number of Ni nearest neighbors of that atom. The system is then a binary alloy from the nuclear-scattering viewpoint, but, magnetically, is a multicomponent alloy with Ni and Mn(n) magnetic atoms. The neutron cross section will accordingly contain terms for all NiMn(n) and Mn(n)Mn(n') atom pairs. We define the magnetic-amplitude difference terms, $\Delta p(n) = p_{Mn(n)} - p_{Ni}$ and $\Delta p(n,n') = p_{Mn(n)} - p_{Mn(n')}$ and write the cross sections as

$$\frac{d\sigma^{\pm}}{d\Omega}(K) = c_{Ni}c_{Mn}\sum_n P(n)[\Delta b \pm \Delta p(n)]^2 S(K,n) + \tfrac{1}{2}c_{Mn}^2\sum_n\sum_{n'} P(n)\,P(n') \times \Delta p(n,n')^2 S(K,n,n'), \quad (8)$$

in which $c_{Mn(n)} = P(n)\,c_{Mn}$, and

$$P(n) = \frac{12!}{n!(12-n)!}\{[1-\alpha(R_1)]c_{Ni}\}^n \times [c_{Mn} + \alpha(R_1)c_{Ni}]^{12-n} \quad (9)$$

is the probability that a Mn atom has n Ni nearest neighbors. The scattering functions are now defined for each of the atom pairs. These are

$$S(K,n) = 1 + 12\,\alpha(R_1,n)\frac{\sin KR_1}{KR_1} + \sum_{i>1} z_i\,\alpha(R_i)\frac{\sin KR_i}{KR_i}. \quad (10)$$

for the NiMn(n) pairs and a similar expression, but with $\alpha(R_1,n,n')$, for the Mn(n)Mn(n') pairs. In this fcc system each atom has 12 nearest neighbors, so the probability of finding a Ni atom at distance R_1 from a Mn(n) atom is just $\frac{1}{12}n$, i.e.,

$$P^{NiMn(n)}(R_1) = \tfrac{1}{12}n, \quad (11)$$

so that

$$\alpha(R_1,n) = 1 - \frac{P^{NiMn(n)}(R_1)}{c_{Ni}} = 1 - n/12\,c_{Ni}. \quad (12)$$

The sum cross section becomes

$$\sum\frac{d\sigma}{d\Omega}(K) = c_{Ni}\,c_{Mn}\sum_n P(n)[\Delta b^2 + \Delta p(n)^2]S(K,n) + \tfrac{1}{2}c_{Mn}^2\sum_n\sum_{n'}P(n)\,P(n') \times \Delta p(n,n')^2 S(K,n,n'), \quad (13)$$

and, to a first approximation, the magnetic terms can be neglected because of the concentration factor in the double sum and since $\Delta b^2 \gg \Delta p(n)^2$. The sum cross section then describes the positional SRO, since $\sum_n P(n)\,S(K,n) = S(K)$. The difference cross section contains only NiMn(n) terms,

$$\Delta\frac{d\sigma}{d\Omega} = 4\,c_{Ni}\,c_{Mn}\,\Delta b\sum_n P(n)\,\Delta p(n)\,S(K,n), \quad (14)$$

and can be expanded to show that the fitted parameters of Table II are related to the model parameters by

$$\Delta p(0) = \sum_n P(n)\,\Delta p(n) = \langle\Delta p\rangle \quad (15)$$

and

$$\alpha(R_1)_{mag} = \Delta p(0)^{-1}\sum_n P(n)\,\Delta p(n)\,\alpha(R_1,n). \quad (16)$$

Although these parameters do not define the moment distribution $\Delta p(n)$, they can be used to test the validity of possible nearest-neighbor models.

For this test we need the nearest-neighbor atomic distributions and the intrinsic Mn and Ni moment values. The atomic distributions are obtained by insertion of the SRO parameters of Table I into Eq. (9), while the Mn and Ni moment values are obtained by combining the neutron data with magnetization data. The neutron data yield

$$\Delta p(0) = \langle\Delta p\rangle = 0.2695\,(\bar{\mu}_{Mn} - \mu_{Ni}), \quad (17)$$

while the mangetization data give

$$\sigma = c_{Mn}\,\bar{\mu}_{Mn} + c_{Ni}\,\mu_{Ni}. \quad (18)$$

TABLE III. Magnetic moments of NiMn alloys at 4.2 °K.

At.% Mn	$\Delta p(0)$[a]	σ[b]	$\bar{\mu}_{Mn}$	μ_{Ni}
5	0.786 ± 0.037	0.73	3.50 ± 0.13	0.584
10	0.715 ± 0.020	0.79	3.18 ± 0.07	0.525
15	0.448 ± 0.014	0.71	2.12 ± 0.05	0.461
20	0.215 ± 0.011	0.46	1.10 ± 0.04	0.300
		± 0.01		± 0.013

[a]Errors include a 10-mb uncertainty in the multiple-Bragg-scattering correction.
[b]Combined magnetization data of Refs. 1–3.

The Ni and average Mn moments are then

$$\mu_{Ni} = \sigma - c_{Mn}[\Delta p(0)/0.2695] \quad (19)$$

and

$$\bar{\mu}_{Mn} = \sigma + c_{Ni}[\Delta p(0)/0.2695]. \quad (20)$$

Here, we neglect conduction-electron polarization (CEP). Previous form-factor studies of ferromagnetic transition metals and alloys generally show a negative CEP with a magnitude of (10–15)% of σ on an atomic volume basis. It is likely that this is also true for NiMn alloys, in which event the μ_{Ni} and $\bar{\mu}_{Mn}$ reported here should be increased by that amount. However, since the CEP has not been measured for the NiMn system and, in any event, is expected to be comparable to the experimental error, we neglect it in this paper. The moment values obtained at 4.2 °K are given in Table III and Fig. 4. These, along with the $P(n)$ values from Eq. (9), allow the calculation of the cross-section parameters for any nearest-neighbor model.

Consider the spin-reversal model, suggested by Carr[6] and subsequently used by other investigators,[13,14] in which those Mn atoms with three or more Mn nearest neighbors have their spins reversed. The $P(n)$ and $\bar{\mu}_{Mn}$ values for the 5%-Mn alloy give an intrinsic Mn moment of $3.5\mu_B$ for this model. The corresponding cross-section parameters are given in Table IV under the column headed Model I. Comparison with the observed parameters shows that this simple spin-reversal model is not consistent with the neutron data and must be discarded. This is contrary to our previous conclusion,[11] which was based on room-temperature data on alloys containing up to 15% Mn and on the assumption that $\mu_{Mn}(T)$ follows the same relative-magnetization curve as the alloy.

The parameters in Table IV require more $\Delta p(0)$ and less $\alpha(R_1)_{mag}$ dependence on Mn content than that given by the spin-reversal model. One way to approach these requirements is to have a net cancellation of the Mn moment produced by fewer Mn first neighbors. Consider, for example, a model in which the ferromagnetic component of the Mn moment is zero for Mn atoms with two or more Mn first neighbors. The $P(n)$ and $\bar{\mu}_{Mn}$ values for the 5%-Mn alloy then yield an intrinsic Mn moment of $3.54\mu_B$. The cross-section parameters for this model appear in Table IV under Model II and are in somewhat better, but still unsatisfactory, agreement with the observed parameters.

From the concentration dependence of these observed and calculated parameters, it appears that the neutron requirements are highly restrictive and that the simple model for which μ_{Mn} is a function of n only will not explain the data. We can force a fit by allowing μ_{Mn} to be a function of both n and concentration. One such fit, which is listed as Model III in Table IV, uses the $\bar{\mu}_{Mn(n)}$-vs-c_{Mn} distribution sketched in Fig. 5. Such a concentration dependence is physically reasonable within the molecular-field framework since the Ni moment, and therefore the effective field at the Mn(n) sites, decreases with increasing Mn content. However,

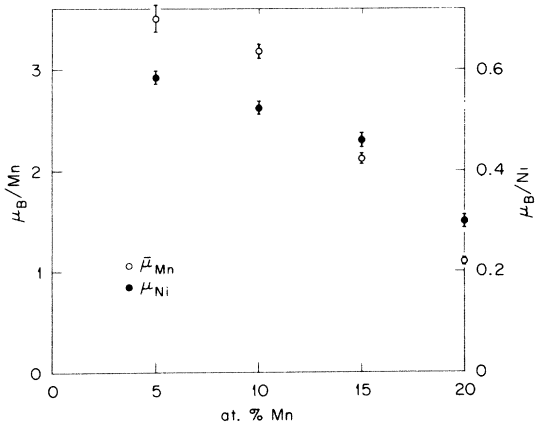

FIG. 4. Concentration dependence of $\bar{\mu}_{Mn}$ and μ_{Ni} at 4.2 °K.

TABLE IV. Comparison of observed and calculated cross-section parameters at 4.2 °K.

$\Delta p(0) = \sum_n P(n)\Delta p(n)$

At.% Mn	Obs.	Model I	Model II	Model III
5	0.786 ± 0.037	0.786	0.786	0.786
10	0.715 ± 0.020	0.745	0.678	0.715
15	0.448 ± 0.014	0.630	0.514	0.448
20	0.215 ± 0.011	0.409	0.367	0.215

$\alpha(R_1)_{mag} = \Delta p(0)^{-1} \sum_n P(n)\Delta p(n)\, \alpha(R_1, n)$

At.% Mn	Obs.	Model I	Model II	Model III
5	−0.04	−0.04	−0.04	−0.04
10	−0.09	−0.07	−0.08	−0.07
15	−0.16	−0.17	−0.15	−0.14
20	−0.25	−0.51	−0.35	−0.24

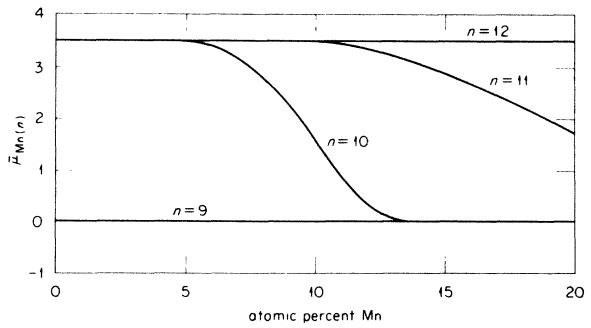

FIG. 5. $\bar{\mu}_{\mathrm{Mn}(n)}$-vs-$c_{\mathrm{Mn}}$ distribution of Model III.

we recognize that this additional functional dependence introduces another level of ambiguity into the model, and that there are probably other physically reasonable models which would also reproduce the neutron-cross-section parameters. We can really only conclude that the ferromagnetic moment of the Mn atoms is strongly dependent on near-neighbor environment, but not simply on the number of nearest-Mn neighbors.

B. Elevated temperatures

In addition to the 4.2 °K data of the previous section we have taken some data at elevated temperatures. The magnetic-cross-section parameters obtained from these data are shown in Table V as a function of the number of SRO parameters included in the fit. Comparison of Tables II and V shows that the $\alpha(R_i)_{\mathrm{mag}}$ parameters are independent of temperature below 10% Mn, but temperature dependent above 10% Mn. This supports the conclusions of the previous section that there are two different regions of magnetic behavior. Below 10% Mn, the binary model is valid and the $\alpha(R_i)_{\mathrm{mag}}$ reflect only the positional SRO, while above 10% Mn the binary model does not apply and the $\alpha(R_i)_{\mathrm{mag}}$ contain additional contributions from magnetic correlations which are temperature dependent.

The individual Mn and Ni moments determined from these parameters are summarized in Table VI, which also includes the relative magnetizations obtained by comparison with the 4.2 °K data. These show a distinctly different thermal behavior for the Mn and Ni moments. At 5% Mn, $\mu_{\mathrm{Ni}}(T)$ follows the same relative-magnetization curve as pure Ni while $\mu_{\mathrm{Mn}}(T)$ decreases more rapidly. Collins and Low[15] also obtained a low Mn moment, $(2.4 \pm 0.1)\mu_B$, from their room-temperature cross-section measurements on NiMn alloys containing less than 3% Mn. They suggested a strong temperature dependence of the Mn moment as a possible mechanism to explain the discrepancy between their result and that obtained from $d\bar{\mu}/dc$. This now appears to be verified. This behavior is also in complete agreement with a previous suggestion by Vincze and Tarnoczi,[16] who based their conclusions on bulk magnetization data.

C. Unpolarized neutrons

We have seen that the polarized-neutron cross-section data do not define the moment distribution and that they are inconsistent with models that attribute the Mn-moment disturbance only to the number of Mn nearest neighbors. This is perhaps not surprising in view of the simplicity of the mod-

TABLE V. Magnetic-cross-section parameters of NiMn alloys at elevated temperatures.

At.% Mn	T (°K)	$\Delta p(0)$	$\alpha(R_1)_{\mathrm{mag}}$	$\alpha(R_2)_{\mathrm{mag}}$	$\alpha(R_3)_{\mathrm{mag}}$	rms dev. (mb)
5	188	0.669	−0.04	−0.01	0.00	1.6
		0.669	−0.04	+0.01		1.6
		0.668	−0.04			1.6
5	298	0.563	−0.05	+0.01	0.00	2.4
		0.563	−0.05	0.00		2.4
		0.564	−0.05			2.4
10	298	0.468	−0.08	−0.07	0.00	2.3
		0.468	−0.08	0.00		2.3
		0.468	−0.08			2.3
15	298	0.286	−0.15	+0.10	−0.02	2.4
		0.286	−0.14	+0.05		2.5
		0.285	−0.13			2.8
20	96	0.186	−0.19	+0.08	0.00	3.2
		0.186	−0.19	+0.08		3.2
		0.185	−0.17			3.6

TABLE VI. Magnetic moments and relative magnetizations at elevated temperatures.

At.% Mn	T (°K)	$\frac{T}{T_c}$	$\sigma(T)$	$\bar{\mu}_{Mn}(T)$	$\mu_{Ni}(T)$	$\frac{\mu_{Mn}(T)}{\mu_{Mn}(0)}$	$\frac{\mu_{Ni}(T)}{\mu_{Ni}(0)}$
5	188	0.33	0.69	3.05 ± 0.13	0.566	0.87 ± 0.05	0.97 ± 0.03
5	298	0.52	0.64	2.63 ± 0.14	0.535	0.75 ± 0.05	0.92 ± 0.03
10	298	0.61	0.61	2.17 ± 0.07	0.436	0.68 ± 0.03	0.83 ± 0.03
15	298	0.75	0.44	1.34 ± 0.05	0.281	0.63 ± 0.03	0.61 ± 0.03
20	96	0.32	0.43	0.98 ± 0.04	0.292	0.89 ± 0.05	0.97 ± 0.06
			± 0.01		± 0.013		

el and the complexity of competing-interaction systems. As an example of a potential complication, consider a Mn atom with three Mn nearest neighbors. There are spatial configurations in which zero, two, or all three of these neighbors are also nearest neighbors of each other. Such spatial configurations could well be important in determining the Mn moment at the origin. There are also magnetic configurations to consider. According to the molecular-field model, a Mn atom with three spin-up Mn neighbors (↑↑↑) would have its spin reversed. However, the same model would not give spin reversal for the configurations (↑↑↓), (↑↓↓), and (↓↓↓). In view of these possible complications within the nearest-neighbor model and the rapidly increasing complexity with more-distant-neighbor models, we have not attempted to extend our calculations to second-neighbor correlations.

The simplest model that will reproduce the cross-section parameters has a net cancellation of the Mn moment with increasing numbers of Mn nearest neighbors and a concentration dependence to the number of neighbors required to produce that cancellation. This cancellation of $\mu_{Mn(n)}$ could arise from averaging over magnetic configurations, from antiferromagnetically coupled spatial configurations, or from a vanishing effective field at the Mn site. Since the neutron parameters contain only NiMn(n) terms and are linear in $\Delta p(n)$, the polarized neutron data cannot distinguish between these, or other, possible cancellation mechanisms.

Additional information is available, in principle, from magnetic disorder scattering of unpolarized neutrons. In the unpolarized-neutron method, one takes the difference between cross sections with the sample unmagnetized and magnetized to saturation parallel to the scattering vector. This difference cross section for the binary model is

$$\Delta \frac{d\sigma}{d\Omega}(K)\bigg|_{\text{unpol}} = \tfrac{2}{3} c(1-c) S(K)\, \Delta p^2 , \tag{21}$$

which, for the NiMn(n) system with nearest-neighbor effects, becomes

$$\Delta \frac{d\sigma}{d\Omega}(K)\bigg|_{\text{unpol}} = \tfrac{2}{3} c_{Ni} c_{Mn} \sum_n P(n)\, \Delta p(n)^2\, S(K,n) + \tfrac{1}{3} c_{Mn}^2 \sum_n \sum_{n'} P(n)\, P(n')\, \Delta p(n,n')^2\, S(K,n,n') . \tag{22}$$

The parameters obtained by fitting to the binary model are related to those of the nearest-neighbor model by

$$\Delta p(0)^2 = \sum_n P(n)\, \Delta p(n)^2 + \frac{1}{2} \frac{c_{Mn}}{c_{Ni}} \sum_n \sum_{n'} P(n)\, P(n')\, \Delta p(n,n')^2 \tag{23}$$

and

$$\alpha(R_1)_{\text{mag}} = \Delta p(0)^{-2} \left[\sum_n P(n)\, \alpha(R_1, n)\, \Delta p(n)^2 + \frac{1}{2} \frac{c_{Mn}}{c_{Ni}} \sum_n \sum_{n'} P(n)\, P(n') \times \alpha(R_1, n, n') \Delta p(n,n')^2 \right] . \tag{24}$$

Since the magnetic-amplitude-difference terms enter quadratically, the parameters will differ for different moment cancellation mechanisms.

We therefore made unpolarized-neutron diffuse-scattering measurements on a NiMn alloy containing 15% Mn. The sample was a polycrystalline cylinder 8 mm in diameter and 3-cm long which had been heat treated in the same way as the plate samples used in the polarized-beam experiments. The measurements were made at 77 °K with a 14-kOe magnetizing field and a neutron wavelength of 1.086 Å. Positional SRO parameters were taken from the field-on cross section and were in substantial agreement with those obtained in the polarized beam experiment. The difference cross section is shown in Fig. 6 along with a fitted curve for the binary model. The corresponding parameters are $\Delta p(0)^2 = 0.56$ and $\alpha(R_1)_{\text{mag}} = -0.08$. These are considerably different from those obtained by Loshmanov[10] at the same composition [$\Delta p(0)^2 = 0.23$ and $\alpha(R_1)_{\text{mag}} \sim 0$]. Although we have no explanation for this large discrepancy, our higher cross section was reproduced both by repeated measurements at 1.086 Å and by data taken in the small-K region with 4.43 Å neutrons. The

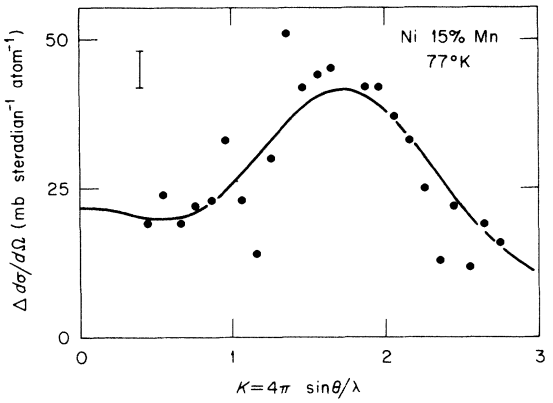

FIG. 6. Unpolarized-neutron magnetic-disorder cross section for a Ni–15-at.%-Mn alloy at 77 °K. Solid curve is a two-parameter fit with parameters $\Delta p(0)^2 = 0.56$ and $\alpha(R_1)_{mag} = -0.08$

parameters calculated for Model III are 0.34 and −0.08, if it is assumed that the ferromagnetic component of the Mn moment vanishes by becoming randomly oriented or by becoming antiferromagnetically coupled. If it is assumed that $\bar{\mu}_{Mn}(n)$ cancels by averaging over up-spin and down-spin magnetic configurations then the parameters for Model III are 0.73 and −0.07. Since these bracket the observed $\Delta p(0)^2$ we are left with the rather unsatisfying conclusion that the magnetic distribution is complicated and not specifically defined by the neutron-cross-section measurements.

IV. SUMMARY AND DISCUSSION

The magnetic behavior of NiMn alloys has long been discussed in terms of a nearest-neighbor molecular-field model with competing interactions. These polarized-neutron results support that model in the sense that near-neighbor magnetic-moment correlations appear in the scattering functions simultaneously with a decrease in the moment difference. However, the neutron cross-sections do not define the moment distribution, but rather provide scattering parameters against which various models can be tested. We have calculated these parameters for a variety of models for which the Mn moment is a function only of the number of nearest-neighbor Mn atoms and find no satisfactory agreement with the observations. We conclude that the moment distribution is more complicated than has previously been assumed and that an additional functional dependence, such as a concentration dependence, is necessary to explain the data. Although the ferromagnetically aligned Mn moment is strongly dependent on near-neighbor environment, that dependence is not simply a matter of the number of Mn nearest neighbors.

The neutron cross sections provide direct information about the concentration and temperature dependence of the Ni and average Mn moments. The thermally saturated, average Mn moment of the 5%-Mn alloy is about $3.5\mu_B$ and, because of the atomic distribution at this concentration level, this should correspond closely to the moment on an isolated Mn atom dissolved in Ni. This is somewhat larger than has generally been assumed, but is in agreement with the more recent magnetization data[3–5] for dilute NiMn alloys. Both the Ni and average Mn moments decrease with increasing Mn content. The μ_{Mn} decrease is apparently associated with a cancellation of the Mn ferromagnetic moment due to near-neighbor environmental effects. Since μ_{Ni} has the same general concentration dependence as μ_{Mn} (see Fig. 4), one is tempted to correlate the Ni-moment reduction with the Mn-moment cancellation. However, μ_{Ni} for the 20%-Mn disordered alloy is nearly the same ($0.3\mu_B$) as that observed[17–19] for the 25%Mn ordered alloy for which there is no Mn-moment cancellation. The Ni-moment reduction with increasing Mn content may be a nonlocal or band effect. Interestingly enough, recent coherent-potential-approximation calculations[20] of the electronic structure of NiMn alloys give results in qualitative aggreement with our conclusions. In those calculations, a moment decrease occurs above 10% Mn, where the majority-spin band begins to intersect the Fermi energy. However, as the authors pointed out, this should be regarded as an averaged effect since

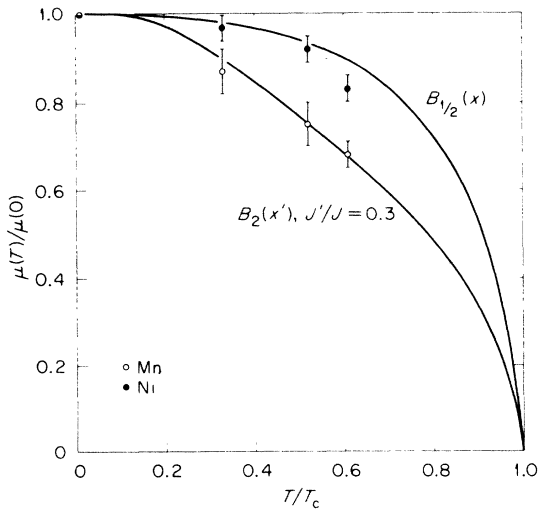

FIG. 7. Relative magnetizations of the Mn and Ni moment of the 5- and 10-at.%-Mn alloys.

the calculations do not take account of local environmental effects which apparently dominate the magnetic behavior of this system.

The Mn and Ni moments exhibit quite different temperature dependences. This type of quasi-independent local-moment behavior has been observed by NMR methods in other alloy systems such as NiCo,[21] FeMn,[22] and NiFe[23] and has been explained[24–26] in terms of virtual spin-wave states. In this model, a weakly coupled impurity will produce a high state density at low energies, so that an increase in temperature leads to a build up of spin disorder at and near the impurity sites. Under these conditions, the magnetization of the impurity is approximately given by the local-moment molecular-field model.

We have used this model to fit the observed relative magnetization of the Mn moments. We define $\epsilon = J_{\mathrm{NiMn}}/J_{\mathrm{NiNi}}$ and assume $S = 2$ and $\frac{1}{2}$ for the Mn and Ni atoms, respectively. The Mn magnetization is then given by the Brillouin function $B_2(y)$, with

$$y = 4\epsilon B_{1/2}(x) T_C/T \ , \tag{25}$$

where

$$x = \tfrac{1}{2} g \mu_B H/k_B T \ . \tag{26}$$

The solid curve in Fig. 7 gives a reasonable representation of the data and corresponds to $B_2(y)$, with $\epsilon = 0.3$. It is interesting that no indication of this behavior was found in the NMR measurements[14] on NiMn alloys for which the Mn^{55} resonance frequency follows the same relative magnetization as the average moment. Comparison with the present data shows that the Mn^{55} hyperfine field is not simply proportional to the local Mn moment.

Finally, we note that the polarized and unpolarized beam methods may give different information. One obtains $\langle \Delta p^2 \rangle$ with unpolarized neutrons and $\langle \Delta p \rangle$ with polarized neutrons. In those systems with pronounced environmental effects, $\langle \Delta p^2 \rangle^{1/2} \neq \langle \Delta p \rangle$, and the polarized method is then required to obtain the average moments of the constituents.

*Research sponsored by the U. S. Atomic Energy Commission under contract with the Union Carbide Corporation.

[1]S. Kaya and A. Kussman, Z. Phys. 72, 293 (1931).
[2]C. Sadron, Ann. Phys. (Paris) 17, 371 (1932).
[3]G. R. Piercy and E. R. Morgan, Can. J. Phys. 31, 529 (1953).
[4]H. C. Van Elst, B. Lubach, and G. J. Van Den Berg, Physica (Utr.) 28, 1297 (1962).
[5]A. V. Doroshenko and S. K. Sidorov, Phys. Met. Metallogr. 21, 169 (1966).
[6]W. J. Carr, Jr., Phys. Rev. 85, 590 (1952).
[7]S. K. Sidorov and A. V. Doroshenko, Phys. Met. Metallogr. 18, 12 (1964).
[8]S. K. Sidorov and A. V. Doroshenko, Phys. Met. Metallogr. 20, 40 (1965).
[9]S. K. Sidorov and A. V. Doroshenko, Phys. Status Solidi 16, 737 (1966).
[10]A. A. Loshmanov, Phys. Met. Metallogr. 18, 22 (1964).
[11]J. W. Cable and H. R. Child, J. Phys. (Paris) Suppl. C 1, 67 (1971).
[12]B. N. Brockhouse, L. M. Corliss, and J. M. Hastings, Phys. Rev. 98, 1721 (1955).
[13]M. J. Marcinkowski and R. M. Poliak, Philos. Mag. 8, 1023 (1963).
[14]R. L. Streever, Phys. Rev. 173, 591 (1968).
[15]M. F. Collins and G. G. Low, Proc. Phys. Soc. Lond. 86, 535 (1965).
[16]I. Vincze and T. Tarnoczi, Solid State Commun. 9, 1239 (1971).
[17]C. G. Shull and M. K. Wilkinson, Phys. Rev. 97, 304 (1955).
[18]A. Paoletti and F. P. Ricci, J. Appl. Phys. 34, 1571 (1963).
[19]A. Delapalme, Solid State Commun. 5, 769 (1967).
[20]H. Hasegawa and J. Kanamori, J. Phys. Soc. Jpn. 33, 1599 (1972).
[21]L. H. Bennett and R. L. Streever, J. Appl. Phys. 33, 1093S (1962).
[22]Y. Koi, A. Tsujimura, and T. Hihara, J. Phys. Soc. Jpn. 19, 1493 (1964).
[23]J. G. Dash, B. D. Dunlap, and D. G. Howard, Phys. Rev. 141, 376 (1966).
[24]V. Jaccarino, L. R. Walker, and G. K. Wertheim, Phys. Rev. Lett. 13, 752 (1964).
[25]H. Callen, D. Hone, and A. Heeger, Phys. Lett. 17, 233 (1965).
[26]T. Wolfram and W. Hall, Phys. Rev. 143, 284 (1966).